The following manuscript was accepted for publication in Pharmaceutical Sciences. It is assigned to an issue after technical editing, formatting for publication and author proofing

Citation: Satish G, Dhayananth N, Kalaichelvi P, Radhakrishnan TK, Karthika S. Determination of chlorzoxazone crystal growth kinetics and size distribution under controlled supersaturation at 293.15 K, Pharm. Sci. 2021, doi: 10.34172/PS.2021.2

Determination of Chlorzoxazone Crystal Growth Kinetics and Size Distribution under Controlled Supersaturation at 293.15 K

G. Satish[1], N. Dhayananth[1], P. Kalaichelvi[1,*], T. K. Radhakrishnan[1], and S. Karthika[2]

[1] Department of Chemical Engineering, National Institute of Technology, Tiruchirappalli – 620015, Tamil Nadu, India

[2] School of Chemical Engineering, Vellore Institute of Technology, Vellore – 632014, Tamil Nadu, India

Abstract

Background: Chlorzoxazone (CHZ) is a water-insoluble drug having bioavailability problems. The absorption rate of such drugs can be improved by reducing their particle size. In this work, the crystal growth kinetics of CHZ–ethanol for different degrees of supersaturation (SS) has been studied.

Method: The equilibrium solubility data of CHZ in ethanol is determined by the shake-flask method within the 283.15–313.15 K temperature range. The mole fraction solubility of CHZ is calculated and correlated with the modified Apelblat equation, λh equation, van't Hoff equation, Wilson, and non-random two liquid (NRTL) equation. Batch crystallization experiments are performed on three different degrees of SS-1.16, 1.18, and 1.20 at 293.15 K as a function of time.

Results: The maximum root mean square difference (RMSD) and relative average deviation (RAD) values of 169.24 $x10^{-6}$ and 0.699 $x10^{-2}$, respectively, are observed in the NRTL equation model. The dissolution properties such as standard enthalpy, standard entropy, and Gibbs free energy are predicted using van't Hoff equation. Using a simple integral technique, the average crystal growth rate constant K_G is calculated as 1.58 (μm/min) $(mg/ml)^{-1}$ and the order n=1 for CHZ–ethanol at 293.15 K.

Conclusion: The obtained result concludes that the crystals growth size is found to be varied at different SS ratio in batch crystallization. The particle size control in batch crystallization can be achieved by optimizing the operating conditions to get the desired size crystals.

Keywords: *Chlorzoxazone, Batch Crystallization, Crystal growth rate, Supersaturation, Crystal size distribution.*

1. Introduction

According to the Biopharmaceutical Classification System (BCS), Chlorzoxazone (CHZ) is a Class II active pharmaceutical drug whose limited dissolution rate leads to the bioavailability problem[1]. CHZ drug is often administered orally and is used as a relaxant and analgesic drug in the treatment of skeletal muscle injuries and pain. Its poor solubility of 0.2–0.3 mg/ml in water has resulted in an extended dissolution rate[2]. The rate of dissolution and absorption of the drug depends on the solubility, permeability, stability, diffusion, and surface area of crystals[3]. Generally, the smaller sized crystals have a faster dissolution rate than the larger sized crystals because of their difference in surface area. In contrast, another study pointed out that a reduction in particle size of crystals has shown a lesser dissolution rate. For example, theophylline drug crystals of size 30–50 µm have shown a faster dissolution rate in comparison to its 10 µm crystals due to agglomeration, thereby reducing its bioavailability[4]. The particle size of crystals is hence an important factor for the circulation of the active therapeutic drug in the bloodstream and to be available at the site of action[4,5].

A uniform particle size distribution of crystals is widely chosen during the process of granulation, compression, capsule filling, and tableting of drugs[6]. The uniform size distribution of the crystals can be produced by carefully controlling the supersaturation (SS) in the crystallizer[7]. Nuclei are formed in the crystallizer containing supersaturated solution by either primary or secondary nucleation. Primary nucleation involves nuclei formed directly from the dissolved solute molecules and is often described by the classical nucleation theory (CNT)[8]. Primary nucleation requires high SS to overcome the resistance and form a new phase, while secondary nucleation can occur even at low SS. There are several methods of crystallization to generate the degree of SS in the solution, such as evaporation, cooling, change of pH, and the addition of anti-solvent[9,10]. Hence, it is a challenge to understand the concept of controlling SS for the desired crystal size distribution. Batch crystallizers are widely employed in industries for the production of fine chemicals and drugs[11,12].

Controlling the degree of SS in the solution is a critical process in the nucleation and growth of crystals[13,14]. Several numerical models have been developed to determine nucleation and crystal growth kinetics of crystals in solution, which are vitally important for crystallization processes. In

batch crystallization operations, nucleation and crystal growth kinetic parameters are derived from the degree of SS at constant temperature[15]. Also, these conditions are often regulated kinetically by other dependent parameters such as temperature, agitation, cooling rate, and micrometric drug properties (i.e., polarity, solubility, stability)[5]. Based on kinetic data applied to the selected model equation, an average crystal growth rate can be calculated which ultimately shows the final distribution of the crystal size. The average crystal size distribution is determined at the end of each run as a function of time for selected SS ratio.

Controlling the degree of SS in crystallization operations can be achieved by developing a metastable zone width region. Nucleation and crystal growth which affect crystallization, cannot take place without SS[16]. To the best of our knowledge, there is no literature available on CHZ kinetic data for the crystal growth rate. The experimental solubility data of the CHZ in ethanol are determined, and their reliability is evaluated through the models viz., modified Apelblat equation, λh equation, van't Hoff equation and Wilson and NRTL model equation[17,18]. The knowledge obtained from the solution's thermodynamic properties is important for predicting a drug's dissolution process in solvent molecules[19]. The apparent thermodynamic properties viz., standard enthalpy, standard entropy, and standard Gibbs free energy in the dissolution process of CHZ-ethanol are calculated using van't Hoff equation. Further, batch crystallization experiments are conducted at different degrees of SS and respective final crystal size distribution as a function of time is determined to estimate the growth rate kinetics.

2. Materials and Methodology

Chlorzoxazone (5-chloro-3H-1,3-benzoxazol-2-one), with the empirical formula $C_7H_4ClNO_2$ (CAS – ID 95-25-0, molar mass-169.56, melting point 191.5ºC, aqueous solubility 0.2-0.3 mg/ml, purity >99.9%), is received as a gift from a manufacturer in Chennai, India. The solvents methanol, and ethanol are purchased with a purity >99.0% from Changshu Hong sheng Fine Chemicals. All the materials used in the research work are of analytical grade and used without further purification.

2.1 Solubility measurements

The solubility value of CHZ-ethanol is calculated for different temperatures from 283.15 K to 313.15 K using the shake-flask method[20]. CHZ drug is added in excess to the test tube containing 2 ml ethanol to obtain the saturated solution, and is placed in a jacketed glass vessel connected to the circulating water bath fitted with a programmable temperature controller. The glass reactor loaded with test tubes is placed on the magnetic stirrer and the contents are stirred using a Teflon coated magnetic pellet. The agitation speed is maintained at 300 rpm for 6 hours at a specified temperature. Then the agitation is stopped, and the saturated solution is allowed to stand 18 hours at the same temperature for settling. Then, 10 µl of the saturated solution is pipetted out carefully from the supernatant solution. The sample is diluted using methanol, and UV-Vis spectroscopy is used to determine the concentration of the dissolved CHZ drug at 283 nm. The same procedure is repeated for other chosen temperatures. Each sample is duplicated during the solubility experiment, and their mean value is taken for further analysis.

2.1.1 Determination of Solubility

A standard stock solution of known concentration is prepared by dissolving CHZ in absolute methanol. The working solutions are prepared at different concentrations in the test tubes and diluted with methanol. The concentration of the working solution is determined by measuring the absorbance read at 283 nm using UV-Vis spectroscopy. As reported in the literature, the UV absorption peak of CHZ is found maximum at 283±2 nm when it is dissolved in absolute methanol[21].

2.2 Metastable Zone width measurements

The metastable zone width of CHZ-ethanol mixture is determined by the polythermal method[22]. Based on the solubility data at respective solubility temperatures, a set of saturated solutions are prepared by dissolving 85,75,65,55 mg/ml CHZ in ethanol. Then, the saturated solution is heated 10 K above the solubility temperature for 30 min with constant agitation of 300 rpm to ensure the complete dissolution of the drug. Now, the clear saturated solution is allowed to cool at a rate of 0.4 K/min. The temperature of the saturated solution is noted when nucleation or cloud point is observed. For all chosen concentrations of drug in equilibrium in the solubility curve, the

procedure is repeated, and all the respective temperatures are marked to establish the metastable region[23].

2.3 Experimental method and determination of crystal growth rate kinetics

The double-jacketed glass crystallizer of volume 100 ml (80mm height x 45 mm width) is used in the present study. The temperature of the glass vessel is maintained using a water bath fitted with a programmable temperature controller. The crystallizer is placed on the magnetic stirrer. Figure 1 displays the experimental setup. The cooling crystallization experiments are performed from 313.15 K to 283.15 K. Hence, the isothermal batch experiments can be performed in the entire cooling range to find the effect of temperature. The initial part of the study is attempted at 293.15 K at different SS to estimate the crystal growth kinetics parameters. The SS ratio of 1.16, 1.18, and 1.20 are chosen at solubility temperature 293.15 K for the experiments. Based on the SS ratio, the solution is prepared in the crystallizer for the desired quantity of CHZ in 30 ml of ethanol. The solution is heated to 303.15 K, above the solubility temperature, where it is allowed to stand for 30 min to ensure the complete dissolution of all crystals. The solution is then allowed to cool at a rate of 0.4 K/min until the set temperature (293.15 K) is reached. The solution is allowed to stand at the same temperature to achieve cloud point nucleation. The time at which the solution turns cloudy indicates the nucleation point and the time is taken as t=0. Then, the samples are withdrawn from the solution using a syringe filter of Polytetrafluoroethylene (PTFE) 0.2 µm size at various time intervals[7]. The concentration of samples is measured at 283 nm using UV-Vis spectroscopy. To measure the mean crystal size, 1 ml of sample is withdrawn simultaneously from the solution at the same time intervals. The crystals are separated from the sample solution through vacuum filtration and are dried in the oven. Since the volume of the solution is 30 ml, only limited number of samples are taken at regular intervals for analyzing particle size distribution. The mean size of crystals is obtained by measuring 100 crystals using the microscopic images taken using an optical microscope (Olympus CX21i)[24]. The Magvision software is used to measure the size of the crystals. The experimental procedure is repeated at various time intervals for all SS ratios to determine the concentration of the solution and the corresponding crystal size distribution.

<Figure 1>

A precise and straight forward technique provided by Rashid et al. has been used in this study to determine the kinetics of crystal growth[7]. In this integral method, the rate of growth was determined by fitting the data on crystal size and SS. The empirical equation used for estimating the growth kinetics is given by equation (1).

$$G = K_G \Delta C^n \qquad (1)$$

In equation (1), G is the linear growth rate (= dL/dt), L is the mean crystal size, 't' is time, $\Delta C = C - C^*$ is SS, where C is the actual solution concentration and C* the equilibrium solution concentration, n, is kinetic order and K_G is the growth rate coefficient[25].

3. Results and Discussion

3.1 Experimental Solubility data of CHZ in ethanol

In a crystallization process, the preciseness in solubility data is important for understanding the concentration of the solute and solvent in thermodynamic equilibrium[23]. Using the shake-flask method, the solubility of CHZ in pure ethanol is determined from 283.15 to 313.15 K[26]. The unknown concentration of CHZ in the solubility experiment is determined from a calibration curve obtained between the known concentrations of CHZ in methanol versus absorbance. A calibration curve of absorbance versus concentration of CHZ in methanol is determined. From the plot, a R^2 value of 0.996 is obtained from the linear fit model. The slope value is used in solubility determination to calculate the unknown concentration of CHZ in the sample.

The mole fraction solubility of the CHZ (x_1) in ethanol is determined using equation (2).

$$x_1 = (m_A / M_A) / (\frac{m_A}{M_A} + \frac{m_B}{M_B}) \qquad (2)$$

In equation (2), m_A and m_B are the masses of the CHZ and ethanol, and M_A and M_B are the molar mass of the CHZ and ethanol respectively. The density of the CHZ (1.5 g/cm^3) and pure ethanol (0.789 g/cm^3) are used to calculate the mole fraction of CHZ in the solution.

3.2 Thermodynamic model parameter estimation

Many thermodynamic solubility models are used to correlate the solid-liquid equilibrium obtained experimentally including activity-coefficient for the solution. The widely used semi-empirical temperature-dependent equations are chosen for the present study to correlate the solubility data such as modified Apelblat, van't Hoff, λh equation, NRTL, and Wilson models. The calculated solubility value obtained from each model are correlated with the experimental solubility data to determine the relative average deviation (RAD) and root mean square deviation (RMSD). Using MATLAB and NCSS Data Analysis software are used to analyze the experimental solubility value of CHZ in pure ethanol, and the model parameter values for the selected thermodynamic models are obtained as explained in the following section.

3.2.1 Modified Apelblat equation

The modified Apelblat equation is a semi empirical equations appropriately used for polar and nonpolar components in the solution. The modified Apelblat equation given by equation (3) is used to correlate the mole fraction solubility and temperature dependence[27,28]

$$\ln x_1 = \mathrm{A} + \frac{\mathrm{B}}{T} + \mathrm{C} \ln T \qquad (3)$$

In equation (3), x_1 is the mole fraction solubility of CHZ in ethanol, T is the absolute temperature (K), and A, B, and C are empirical parameters. The equation contains three adjustable parameters which is modified from the simplified Apelblat equation which contains only two parameters[29]. The values of A and B shows the variation in activity coefficients in the solution, and C shows the effect of temperature on the fusion enthalpy as a deviation of heat capacity.

3.2.2 λh Equation

The λh equation is a semi-empirical equation (4) and is used for the fitness of experimental data on solubility[30,31]. This equation is used to study the hydrogen bonding solute solubility and solvent interactions along the line of saturation with temperature[17]

$$\ln\left(1 + \lambda \frac{1-x_1}{x_1}\right) = \lambda h \left(\frac{1}{T} - \frac{1}{T_{m1}}\right) \qquad (4)$$

In equation (4), x_1 is the mole fraction solubility of CHZ, and T and T_{m1} are temperature and melting temperature of CHZ in Kelvin. The λ and h are the two adjustable parameters, where λ represents the non-ideality of the solution system, and h denotes the enthalpy of the solution.

3.2.3 van't Hoff Equation

The van't Hoff equation is an ideal equation which is used to determine the temperature dependence solubility of solid-liquid equilibrium. Equation (5) is also used to predict values of enthalpy, entropy and Gibbs free energy for the real solution. This gives the empirical relationship between the mole fraction solubility of solute and the respective temperature in real solution[30,32]

$$\ln x_1 = -\frac{\Delta H_d}{RT} + \frac{\Delta S_d}{R} \qquad (5)$$

where x_1 is the mole fraction solubility of CHZ, T is temperature, and R is the universal gas constant. ΔH_d and ΔS_d represent the standard enthalpy and standard entropy, respectively.

3.2.4 Wilson Model

It is a semi-empirical equation and also called as activity coefficient model. The equation is used to measure the activity coefficient for a solid-liquid system at a given pressure and temperature. It also an example of local composition model mainly used to determine the cross interaction energy parameters for respective solute-solvent system[30]. For a binary solute-solvent system, the logarithm of solute activity coefficient described is given by equation (6)[17,32]

$$\ln \gamma_1 = -\ln(x_1 + \Lambda_{12}x_2) + x_2\left[\frac{\Lambda_{12}}{x_1+\Lambda_{12}x_2} - \frac{\Lambda_{21}}{x_2+\Lambda_{21}x_1}\right] \qquad (6)$$

where $\Lambda_{12} = \frac{V_2}{V_1} exp\left(\frac{\Delta\lambda_{12}}{RT}\right)$ and $\Lambda_{21} = \frac{V_1}{V_2} exp\left(\frac{\Delta\lambda_{21}}{RT}\right)$.

In equation (6), $\Delta\lambda_{12}$ and $\Delta\lambda_{21}$ are the cross interaction energy parameters that can be fitted with experimental solubility data and V_1 and V_2 are the molar volume of solute and solvent which are the adjustable parameters with temperature. x_1 and x_2 are the mole fraction of the solute and solvent.

3.2.5 Non-random two-liquid model (NRTL)

NRTL model is widely used to describe the solid-liquid equilibrium. It is used to correlate the activity coefficients γ_i of a compound with its mole fractions x_i in the liquid phase. The concept of NRTL is to determine the non-randomness at local molecular level in non-ideal solution and so called as local composition model[30,32]. The NRTL model proposed by Renon and Prausnitz contains three parameters per binary interaction, compared with the two parameters of the Wilson model. The activity coefficient of this model can be expressed using the equation (7)[4,17,28]

$$\ln \gamma_1 = x_2^2 \left[\frac{\tau_{21} G_{21}^2}{(x_1 + G_{21} x_2)^2} - \frac{\tau_{12} G_{12}}{(x_2 + G_{12} x_1)^2} \right] \qquad (7)$$

In equation (7), G_{12}, G_{21}, τ_{12}, and τ_{21} are the model parameters and can be determined, where

$$G_{12} = \exp(-\alpha_{12}\tau_{12})$$

$$G_{21} = \exp(-\alpha_{21}\tau_{21})$$

$$\tau_{12} = \frac{\Delta g_{12}}{RT}$$

$$\tau_{21} = \frac{\Delta g_{21}}{RT}$$

where, Δg_{12} and Δg_{21} are the cross-interaction energy parameters that can be fitted by experimental solubility data, and α is the parameter related to the randomness of the mixture with $\alpha_{12} = \alpha_{21}$. α is also an adjustable parameter which can be fitted by experimental solubility data together with Δg_{12} and Δg_{21}.

The models viz, modified Apelblat equation, λh equation, van't Hoff equation, Wilson, and NRTL equation considered in this investigation are compared with concentration values derived from the solubility experiments. For all models, the values of parameters derived by curve fitting in MATLAB are reported in Table 1 along with the respective RAD and RMSD. The reliability of all parameters estimated through MATLAB is determined by repeating the parameter estimation using NCSS Data Analysis software. The discrepancy between the calculated values is very negligible for both tools. The models with the estimated parameters are used to calculate the

solubility data and compared with the experimental solubility data of the present investigation. Table 2 lists the experimental solubility value for temperature 283.15 to 313.15 K together with the calculated values obtained from the modified Apelblat equation, λh equation, van't Hoff equation, Wilson equation, and NRTL equation and their respective relative deviation.

The solubility error difference between the calculated and the experimental values are calculated by relative deviation (RD), RAD, and RMSD using equations (8), (9), and (10) respectively.

$$\text{RD} = \left(x^{exp} - \frac{x^{cal}}{x^{exp}}\right) \quad (8)$$

$$\text{RAD} = \frac{1}{\text{N}} \sum\left(x^{exp} - \frac{x^{cal}}{x^{exp}}\right) \quad (9)$$

In equation (8), N is the number of experimental points, x^{exp} and x^{cal} are the mole fraction values of experimental solubility and calculated solubility respectively.

$$\text{RMSD} = \left[\frac{1}{\text{N}}\sum\left(x^{exp} - \frac{x^{cal}}{x^{exp}}\right)^2\right]^{\frac{1}{2}} \quad (10)$$

The parameters calculated for the selected thermodynamic models and their acquired values are listed in Table 1, together with RAD and RMSD.

<Table 1>

The calculated RAD values among the models are found to be less than 3% with a smaller RMSD value, which indicated that selected models could be comfortably adapted to the experimental values. However, from the NRTL model equation (Table 1), the RMSD value of 169.24 $x10^{-6}$ and the RAD value of 0.699 $x10^{-2}$ are found to be lower than other thermodynamic models chosen in the present study. The NRTL equation is found to be more accurate than the other model equations selected for the present study in order to correlate the solubility results of the CHZ–ethanol system. These results concluded that the solubility values obtained from the experiments can be used as essential data for designing and optimizing the experimental process of CHZ crystallization.

<Table 2>

The experimental mole fraction solubility value of CHZ in pure ethanol and calculated solubility values for selected thermodynamic models are compared. The RD are found to be least between the experimental and calculated solubility values of selected models shown in Table 2. It is observed that the solubility of CHZ drug increases, corresponding to the rise in temperatures selected in the present study.

3.3 Apparent thermodynamic properties for the solution

The thermodynamic properties of the system viz., enthalpy, and entropy are determined by the van't Hoff equation. Figure 2 illustrates van't Hoff plot of the logarithm of mole fraction solubility versus the reciprocal of absolute temperature. From the plot of the linear curve, a significant R^2 of 0.99 was obtained and hence data obtained from the plot are found to be reliable. The slope and intercept values determine the dissolution enthalpy and entropy respectively[32].

<Figure 2>

The Gibbs free energy of the solution is calculated using equation (10)[32]

$$\Delta G_{\mathrm{d}} = \Delta H_{\mathrm{d}} - T\Delta S_{\mathrm{d}} \qquad (10)$$

In equation (10), ΔG_{d} is the Gibbs free energy of the dissolution process. Thermodynamic properties of enthalpy, entropy, and Gibbs energy values are calculated and listed in Table 3. The results show positive values ($\Delta H_{\mathrm{d}} > 0$), which indicated that the dissolution process of CHZ in ethanol is endothermic. The values of ΔH_{d} showed that the enthalpy of the dissolution process is a linear function of temperature where the heat capacity of the solution is constant[32]. The values of entropy are higher than the enthalpy of the dissolution process to overcome the cohesive force of interaction between the solute and solvent molecules[33]. The entropy (ΔS_{d}) value is found to be positive, and it is the driving force for the dissolution process of the CHZ and ethanol system. The values of ΔG_{d} for the system are positive, and the value decreases with an increase in the temperature of the solution. The variation in Gibb's free energy values denotes the dissolution process in which the smaller value of ΔG_{d} has stronger dissolving power. From the values, it can

be inferred that a smaller value of Gibb's free energy is obtained with an increase in temperature which showed the experimental values having a stronger dissolving process.

<Table 3>

<Figure 3>

<Figure 4>

3.4 Metastable Zone Width Measurements

The metastable zone width of CHZ in ethanol is determined using the polythermal method at 0.4 K/min cooling rate and is shown in Figure 3. The metastable zone is developed from the selected concentration of CHZ 85, 75, 65, and 55 mg/ml. In the present study, three different ratios of SS-1.16, 1.18, and 1.20 are selected as shown in Table 4. The selection of SS is based on the region between solubility curve and metastable zone curve. At 293.15 K, three different points are chosen in order to estimate the crystal growth kinetics between higher SS and lower SS region. The SS-1.16 is found just above the solubility curve and SS-1.20 is found just below metastable zone curve. An intermediate SS-1.18 is also chosen. At low SS, the nucleation is slower, whereas, at high SS region, the nucleation is found to be faster and hence depletion of solute concentration is faster[34]. The region of metastable zone width is the ideal zone for the crystal growth once the nuclei are formed[35]. Crystal growth is observed from pre-existing nuclei in the region of SS (i.e., solute concentration is more than the solubility). The crystal growth is slow for the lower SS, which ultimately produces on larger sized crystals as crystallization proceeds. The size distribution of crystals at three selected SS ratio is determined by batch crystallization experiments operated at 293.15 K. The results of three different degrees of SS and their respective mean crystal size distribution and the final concentration of the solution are shown in Table 4. The dried crystals are used for image analysis to determine the average crystal size distribution. The images are taken and then size is measured for the sample of 100 crystals using optical microscopy connected with Magvision software and are shown in Figure 4a and 4b**.**

<Table 4>

<Figure 5>

<Figure 6>

<Figure 7>

In a crystallization process, nucleation and growth continue to occur simultaneously. SS is the driving force of the crystallization; and the rate of nucleation and growth is driven by the existing SS in the solution[10]. Depending upon the conditions, either nucleation or growth may be predominant over the other. The SS is higher at the initial stages and hence the birth of new nuclei is faster. After that, the crystals which achieve the critical crystal size start to grow fast since the remaining SS is utilized for growth. The crystal growth will reduce the solution concentration and hence the SS also reduces. When the SS falls, the crystal growth also starts reducing and becomes stable in later stages of crystallization.

It could be observed from Figures 5, 6 and 7 that the concentration of the solution decreases with time as the crystallization proceeds. It is observed from the data that the crystal nucleation begins around 40 min when the SS is 1.16. But, when the SS increases, the time at which nucleation starts decreases to 10 min. This is due to the higher rates of collision that occur at higher solution concentrations. From Figure 5a and 7a, it is understood that the growth of the crystals is faster initially and then it decreases as the crystallization proceeds. The decrease in the growth rate is due to the decrease in the solute concentration as time increases. The mean size of the crystals measured near the nucleation points for three different SS- 1.16, 1.18, 1.2 are found to be 324±102.24 µm, 181±80.19 µm and 359±89.63 µm respectively. The mean size at the end of the crystallization is 815±105.23 µm, 476±117.20 µm and 595±113.44 µm respectively for three different SS ratios.

In higher SS, the number of nucleating particles is more initially than in a lower SS. Further, as time progresses in batch crystallization, the solute concentration in the solution decreases which affects the nucleation and the growth of crystals is limited. Similarly, results showed in SS-1.18 that the more nucleated particles grow eventually, and the mean size of crystals at the end of the crystallization is found to be 476±117.20 µm. In case of SS-1.16 the mean size of crystal at the

end of crystallization is 815±105.23 µm which is found to be larger than SS 1.18 and SS 1.20. In lower SS-1.16 number of nucleating particles is less and the decrease in solute concentration is also slower. In addition, the possibility of critical nuclei (unstable nuclei) that tend to adhere over the surface of larger crystals or quickly incorporated in stable crystal lattice rather than grow into a new crystal[36]. Hence, at lower SS-1.16, the size enlargement of the crystals is of relatively larger size and so SS-1.16 shows the variation in the mean average size of crystals than other SS (1.18 and 1.20). The results have concluded that at different SS the growth size of crystals varied during batch crystallization. The physical factors like solution stirring (rpm) shows its effect resulting the crystal polydispersity. The control of the particle size in batch crystallization can be achieved by optimizing the operating condition to obtain desired size crystals.

<Table 5>

3.5 Crystal growth kinetics

During the experimental runs, it is observed that the growth rate of crystals is directly proportional to the SS of the solution. The relationship between SS and growth rate of crystals is an important parameter to determine the growth rate constant[37]. Equation (1) is an empirical power law equation that describes the relationship between the growth rate of crystal and the SS. The plot of log G vs log ΔC gives the values of order (n) and growth rate constant (K_G). The slope of the line gives the order (n) of crystal growth and the intercept yields a growth rate constant (K_G). The results indicated that the order of crystal growth n~1 and growth rate constant K_G is 1.58 (µm/min) $(mg/ml)^{-1}$ of CHZ-ethanol at 293.15 K with the least deviations as shown in Table 5. The growth rate-limiting step can be identified from the value of the order which usually lies between 1 and 2. More specifically, the value of n=1 means that diffusion of the crystallizing molecules to the crystal surface is the rate-limiting step. The value of n=2 means that the incorporation of crystallizing molecules in the crystalline lattice is the rate-limiting step[38]. Similarly, the order value (n~1) is found for each SS ratio, it indicates that the growth rate of the crystal is limited by the diffusion of the solute molecules to the crystal surface. Thus, the results indicate that growth rate is a function of the initial SS which determines crystal size distribution in the crystallization operations.

4. Conclusion

The CHZ solubility in pure ethanol is determined using the shake-flask technique at various temperatures ranging from 283.15 to 313.15 K. The experimental results suggest that CHZ solubility in ethanol is a function of temperature. The experimental solubility data is correlated using the modified Apelblat equation, λh equation, van't Hoff equation, Wilson, and NRTL equation. The results of the correlation show that mole fraction solubility values obtained from the NRTL equation are close to that of the experimental mole fraction solubility values of CHZ in ethanol. Hence, the NRTL equation is more accurate in describing the solubility data compared with other models. Using the van't Hoff equation, the values obtained for enthalpy, entropy are found to be positive and hence the dissolution process of CHZ-ethanol is endothermic. The Gibbs free energy values are found to be smaller when raises in temperature, which suggested that CHZ-ethanol has stronger dissolving power. The results of the batch crystallization experiments are carried out for three different SS ratios (SS-1.16, 1.18, and 1.20) operated at 293.15 K demonstrates that the higher concentration (SS-1.20) have a rapid growth of crystals than of lower concentrations. The crystal growth rate is slower for lower concentration (SS-1.16), but relatively large size crystals are observed at end of the experiments. An empirical equation is used to estimate the kinetic growth rate K_G is 1.58 (μm/min) $(mg/ml)^{-1}$ and order n~1. The findings enable us to conclude that optimizing the SS is important to obtain the desired crystal size distribution.

Declarations

Funding– Not Applicable

Conflicts of Interest/ Competing interests- The authors report no conflicts of interest.

Authors' Contribution- The authors have equally contributed towards the research work

5. References

1. Raval MK, Patel JM, Parikh RK, Sheth NR. Dissolution enhancement of chlorzoxazone using cogrinding technique. Int J Pharm Investig. 2015;5(4):247. doi: 10.4103/2230-973x.167689

2. Thakore KN, Mehendale HM. Chlorzoxazone. In: Encyclopedia of Toxicology. 2014. p. 938.

3. Khadka P, Ro J, Kim H, Kim I, Kim JT, Kim H, et al. Pharmaceutical particle technologies: An approach to improve drug solubility, dissolution and bioavailability. Asian J Pharm Sci. 2014;9(6):304–16. doi: 10.1016/j.ajps.2014.05.005

4. Sun J, Wang F, Sui Y, She Z, Zhai W, Wang C, et al. Effect of particle size on solubility, dissolution rate, and oral bioavailability: Evaluation using coenzyme Q10 as naked nanocrystals. Int J Nanomedicine. 2012;7:5733. doi: 10.2147/ijn.s34365

5. Patience DB, Rawlings JB. Particle-shape monitoring and control in crystallization processes. AIChE J. 2001;47(9):2125–30. doi: 10.1002/aic.690470922

6. Chen J, Sarma B, Evans JMB, Myerson AS. Pharmaceutical crystallization. Cryst Growth Des. 2011;11(4):887–95. doi: 10.1021/cg101556s

7. Rashid A, White ET, Howes T, Litster JD, Marziano I. Growth rates of ibuprofen crystals grown from ethanol and aqueous ethanol. Chem Eng Res Des. 2012;90(1):158–61. doi: 10.1016/j.cherd.2011.08.003

8. Karthika S, Radhakrishnan TK, Kalaichelvi P. A Review of Classical and Nonclassical Nucleation Theories. Cryst Growth Des. 2016;16(11):6663–81. doi:10.1021/acs.cgd.6b00794

9. Luft JR, Detitta GT. Kinetic aspects of macromolecular crystallization. Methods Enzymol. 1997;276:110–31. doi: 10.1016/s0076-6879(97)76053-1

10. Vedantam S, Ranade V V. Crystallization: Key thermodynamic, kinetic and hydrodynamic aspects. Sadhana. 2013;38(6):1287–337. doi: 10.1007/s12046-013-0195-4

11. Tavare NS. Batch Crystallizers: a Review. Chem Eng Commun. 1987;61(1–6):259–318. doi: 10.1080/00986448708912042

12. Mayrhofer B, Nývlt J. Programmed cooling of batch crystallizers. Chem Eng Process.

1988;24(4):217–20. doi: 10.1016/0255-2701(88)85005-0

13. Zhou Y, Kovenklioglu S. Growth and nucleation kinetics in batch crystallization of triclosan. Chem Eng Commun. 2004;191(6):749–66. doi: 10.1080/00986440490275705

14. Li H, Kawajiri Y, Grover MA, Rousseau RW. Modeling of Nucleation and Growth Kinetics for Unseeded Batch Cooling Crystallization. Ind Eng Chem Res. 2017;56(14):4060–73. doi: 10.1021/acs.iecr.6b04914

15. Fevotte G, Klein JP. A new policy for the estimation of the course of supersaturation in batch crystallization. Can J Chem Eng. 1996;74(3):372–84. doi: 10.1002/cjce.5450740308

16. Mitchell NA, Óciardhá CT, Frawley PJ. Estimation of the growth kinetics for the cooling crystallisation of paracetamol and ethanol solutions. J Cryst Growth. 2011;328(1):39–49. doi: 10.1016/j.jcrysgro.2011.06.016

17. Zhao X, Han G, Zhao H. Thermodynamic Solubility and Mixing Properties of Phenformin in 14 Pure Solvents at Temperatures Ranging from 278.15 to 323.15 K. J Chem Eng Data. 2019;64(12):6009–19. doi: 10.1021/acs.jced.9b00844

18. Wang K, Hu Y, Yang W, Guo S, Shi Y. Measurement and correlation of the solubility of 2,3,4,5- tetrabromothiophene in different solvents. J Chem Thermodyn. 2012;55:50–5. doi: 10.1016/j.jct.2012.06.005

19. Liang R, Bao Z, Su B, Xing H, Ren Q. Solubility of vitamin D3 in six organic solvents at temperatures from (248.2 to 273.2) K. J Chem Eng Data. 2012;57(8):2328–31. doi: 10.1021/je300401c

20. Baka E, Takács-Novák K. Study on standardization of shake-flask solubility determination method. Eur J Pharm Sci. 2007;32(1):S23–4. doi: 10.1016/j.ejps.2007.05.048

21. Stewart JT, Janicki CA. Chlorzoxazone. In: Analytical Profiles of Drug Substances. Elsevier; 1987. p. 119–44.

22. Mitchell NA, Frawley PJ. Nucleation kinetics of paracetamolethanol solutions from

metastable zone widths. J Cryst Growth. 2010;312(19):2740–6. doi: 10.1016/j.jcrysgro.2010.05.043

23. Zeng G, Li H, Huang S, Wang X, Chen J. Determination of metastable zone width and the primary nucleation kinetics of sodium sulfate. Theor Found Chem Eng. 2015;49(6):869–76. doi: 10.1134/s0040579515050309

24. Alander EM, Uusi-Penttila MS, Rasmuson AC. Characterization of paracetamol agglomerates by image analysis and strength measurement. Powder Technol. 2003;130(1–3):298–306. doi: 10.1016/s0032-5910(02)00208-5

25. Karpiński PH. Crystallization as a mass transfer phenomenon. Chem Eng Sci. 1980;35(11):2321–4. doi: 10.1016/0009-2509(80)87010-2

26. Baka E, Comer JEA, Takács-Novák K. Study of equilibrium solubility measurement by saturation shake-flask method using hydrochlorothiazide as model compound. J Pharm Biomed Anal. 2008;46(2):335–41. doi: 10.1016/j.jpba.2007.10.030

27. Yan F-Y, Wang M, Wen J-Y, Fu Y, Chen L. Solubility of Fudosteine in Some Pure and Mixed Solvents from (278.15 to 308.15) K. J Appl Solut Chem Model. 2012;1(2):100–4. doi: 10.6000/1929-5030.2012.01.02.4

28. Qing X-Y, Fu H-L, Shu G, Liu M-J, Zhou J-Y, Wu W-B, et al. Solubility and solution thermodynamics of diphenoxylate in different pure solvents. J Chem Eng Data. 2015;60(6):1629–33. doi: 10.1021/je5010033

29. Jin S, Cui X, Qi Y, Shen Y, Li H. Measurement and correlation of the solubility of β-Cyclodextrin in different solutions at different temperatures and thermodynamic study of the dissolution process. Processes. 2019;7(3). doi: 10.3390/pr7030135

30. Chen J, Zeng ZX, Xue WL, Wang D, Huang Y. Determination and correlation of solubility of decahydropyrazino[2,3-b] pyrazine in methanol, ethanol, and 2-propanol. Ind Eng Chem Res. 2011 Oct 19;50(20):11755–62. doi: 10.1021/ie2012714

31. Noubigh A, Oueslati MH. Measurement and modeling of the solubility of vanillin constituent of olive mill wastewater in binary water+ ethanol solvents mixtures between 278.15 K and 308.15 K, Aust. J Basic Appl Sci. 2014;8:396–403.

32. Tao M, Wang Z, Gong J, Hao H, Wang J. Determination of the solubility, dissolution enthalpy, and entropy of pioglitazone hydrochloride (form II) in different pure solvents. Ind Eng Chem Res. 2013;52(8):3036–41. doi: 10.1021/ie303588j

33. Zhang F, Tang Y, Wang L, Xu L, Liu G. Solubility determination and thermodynamic models for 2-methylnaphthalene in different solvents from T=(278.15 to 303.15) K. J Chem Eng Data. 2015;60(6):1699–705. doi: 10.1021/je5010627

34. Lindfors L, Forssén S, Westergren J, Olsson U. Nucleation and crystal growth in supersaturated solutions of a model drug. J Colloid Interface Sci. 2008;325(2):404–13. doi: 10.1016/j.jcis.2008.05.034

35. Parsons AR, Black SN, Colling R. Automated measurement of metastable zones for pharmaceutical compounds. Chem Eng Res Des. 2003;81(6):700–4. doi: 10.1205/026387603322150552

36. Nanev CN. Relationship between number and sizes of crystals growing in batch crystallization: Nuclei number density, nucleation kinetics and crystal polydispersity. J Cryst Growth. 2020;546:125786. doi: 10.1016/j.jcrysgro.2020.125786

37. O Ciardha CT, Mitchell NA, Hutton KW, Frawley PJ. Determination of the Crystal Growth Rate of Paracetamol As a function of solvent composition. Ind Eng Chem Res. 2012;51(12):4731–40. doi: 10.1021/ie2020262

38. Alonzo DE, Raina S, Zhou D, Gao Y, Zhang GGZ, Taylor LS. Characterizing the impact of hydroxypropylmethyl cellulose on the growth and nucleation kinetics of felodipine from supersaturated solutions. Cryst Growth Des. 2012;12(3):1538–47. doi: 10.1021/cg201590j

LIST OF FIGURES

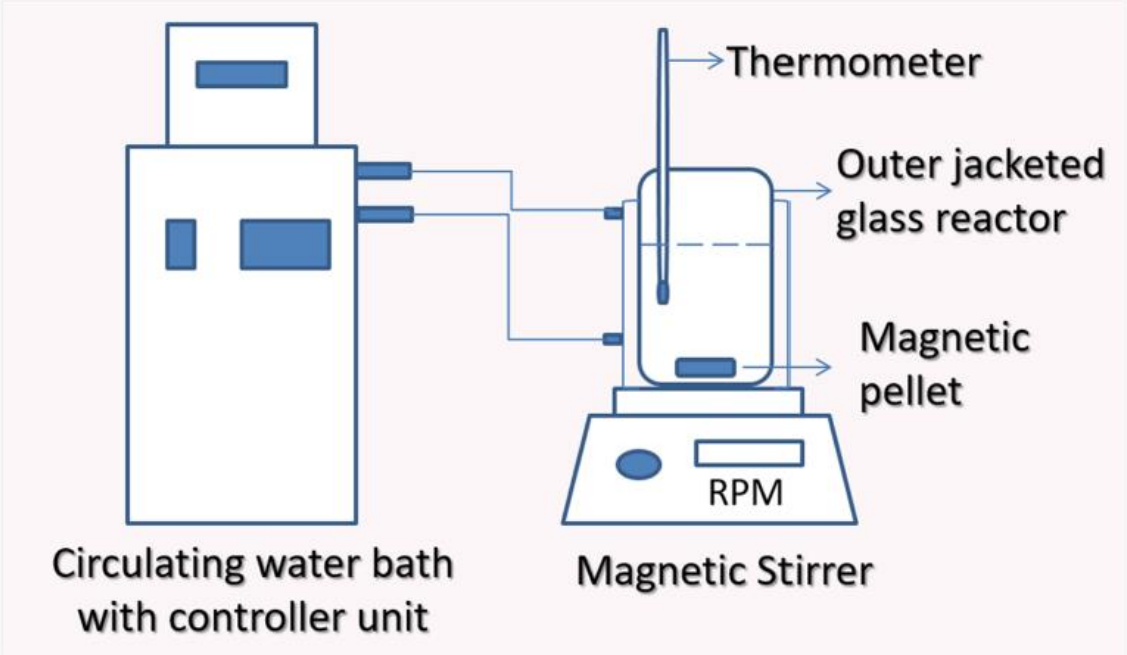

Figure 1: Schematic representation of experimental setup

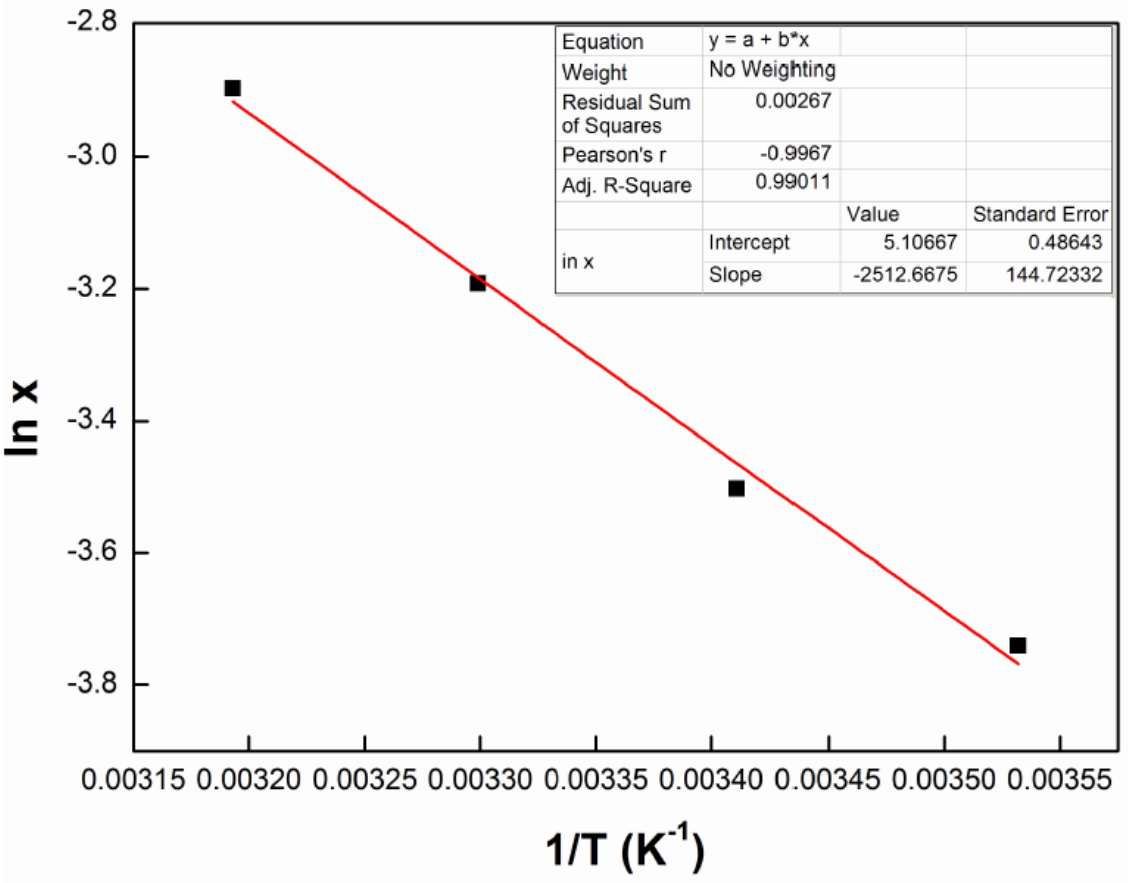

Figure 2: van't Hoff plot of mole fraction the solubility of CHZ

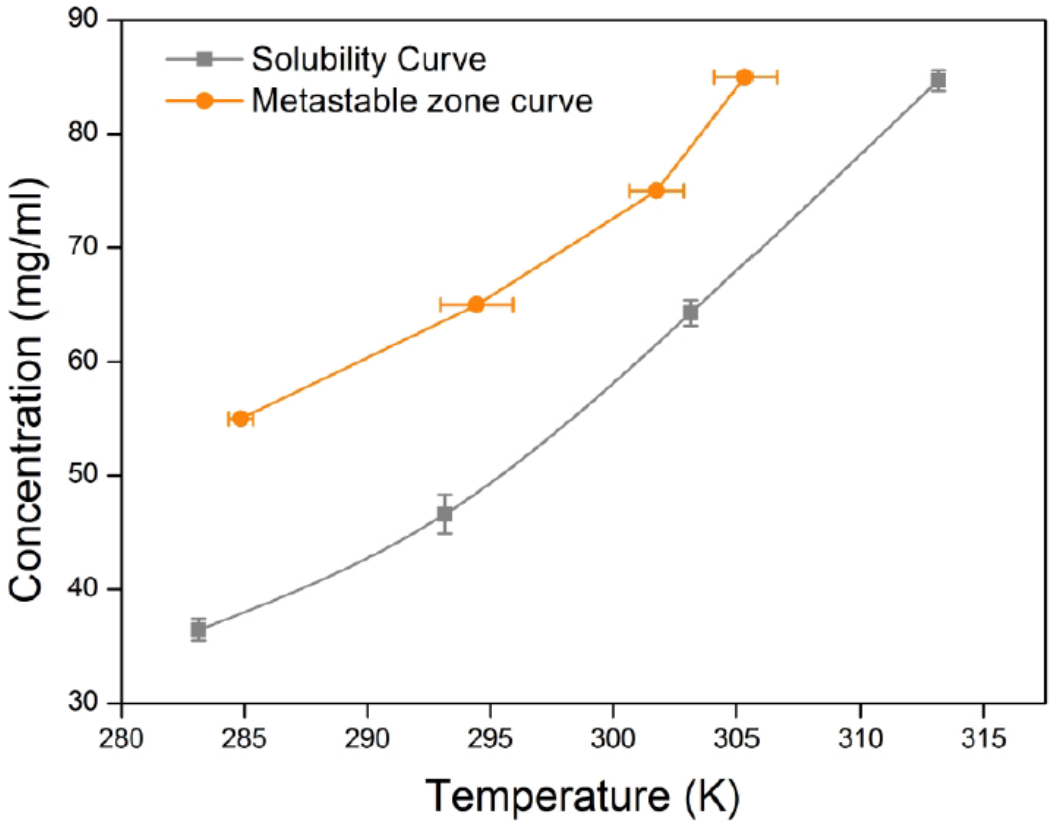

Figure 3: Solubility and Metastable Zone width for CHZ-Ethanol

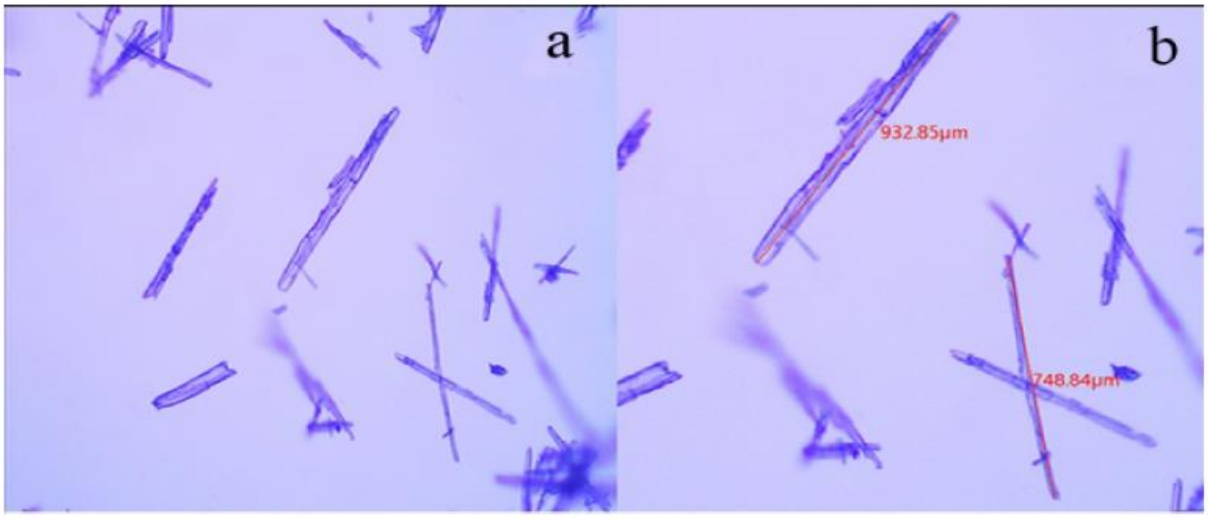

Figure 4: Optical image taken for a) sample between the time intervals b) crystal size measurement

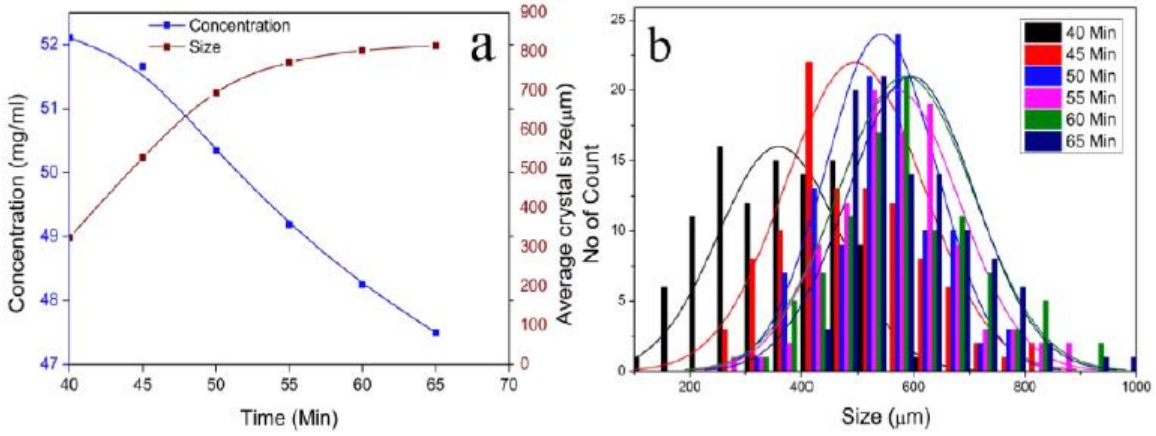

Figure 5: Solution concentration and average crystal size of a) SS-1.16 b) Crystal size distribution of SS-1.16

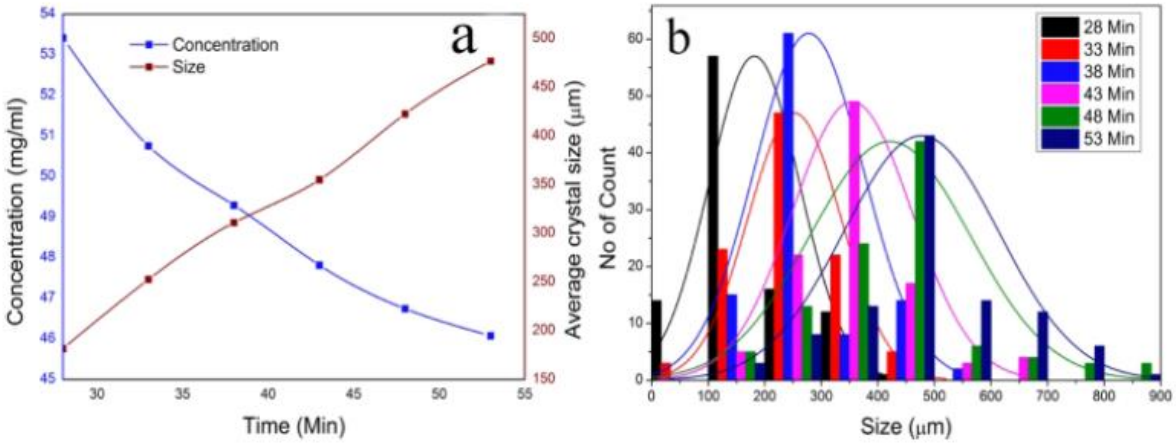

Figure 6: Solution concentration and average crystal size of a) SS-1.18 b) Crystal size distribution of SS-1.18

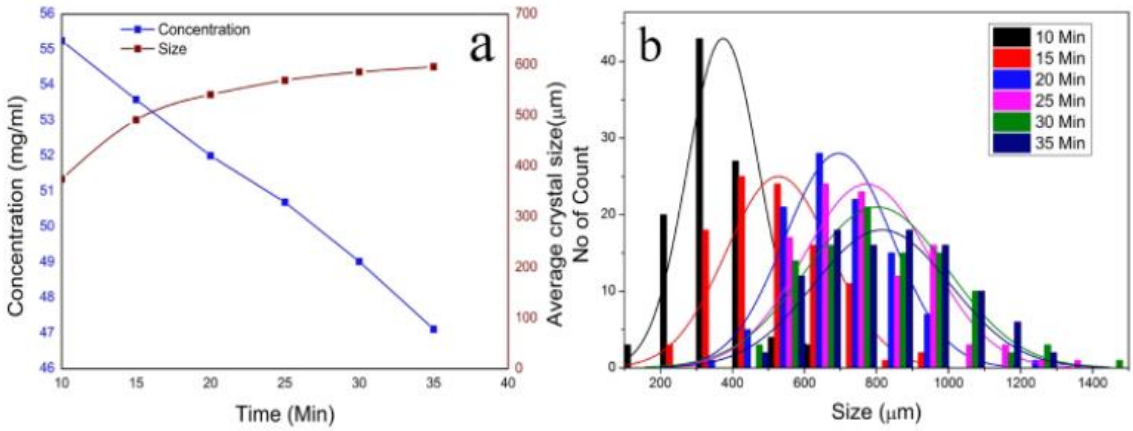

Figure 7: Solution concentration and average crystal size of a) SS-1.20 b) Crystal size distribution of SS-1.20

Table 1: Parameters of the model equation for CHZ in ethanol

Model Equation	Parameters	Values	100 RAD	10^6 RMSD
Apelblat	A	-54.85	2.004	345.05
	B	14.12		
	C	8.922		
λh	*λ*	0.4099	2.388	407.69
	h	6300.07		
van't Hoff	ΔH_d (kJ/mol)	21.29	2.507	427.37
	ΔS_d (J/mol.K)	38.49		
Wilson	λ_{12}	-3467.806	2.533	456.56
	λ_{21}	90619.64		
NRTL	A	0.1159015	0.699	169.24
	g_{12}	-12527.58		
	g_{21}	24427.24		

Table 2: Mole fraction solubility of CHZ in ethanol from temperature 283.15 to 313.15 K

T/K	Experimental Solubility Value (x_1)	Calculated solubility values (x)									
		Modified Apelblat	RD	λh	RD	van't Hoff	RD	Wilson	RD	NRTL	RD
283.15	0.0124±0.96	0.01192	0.040	0.01184	0.047	0.01181	0.050	0.01188	0.044	0.01244	-0.002
293.15	0.0158±1.70	0.01622	-0.025	0.01627	-0.028	0.01627	-0.029	0.01638	-0.035	0.01599	-0.0122
303.15	0.02166±1.12	0.02184	-0.008	0.02193	-0.012	0.02195	-0.013	0.02212	-0.021	0.02157	0.004
313.15	0.02931±0.91	0.02914	0.005	0.02907	0.008	0.02906	0.008	0.02933	-0.005	0.02906	-0.008

Table 3: Predicted values of dissolution Enthalpy, Entropy and Gibbs free energy

Properties of solution	Temperature (K)			
	283.15	**293.15**	**303.15**	**313.15**
ΔH_d(kJ/mol)	21.29	21.29	21.29	21.29
ΔS_d(J/mol.K)	38.49	38.49	38.49	38.49
ΔG_d(kJ/mol)	10.4	10.01	9.6	9.2

Table 4: SS concentration at 293.15 K at respective time intervals and average crystal size distribution of CHZ

Supersaturation Ratio	Initial Concentration (mg/ml)	Sampling time interval (min)	Average crystal size (µm)	Final concentration (mg/ml)
1.16	54	40	324.92±102.24	52.11
		45	528.64±98.80	51.66
		50	695.35±84.11	50.34
		55	772.28±95.12	49.19
		60	802.87±97.94	48.25
		65	815.77±105.23	47.5
1.18	55	28	181.59±80.19	53.41
		33	252.57±82.01	50.75
		38	310.87±96.67	49.29
		43	354.41±105.77	48.81
		48	422.52±115.25	47.74
		53	476.70±117.20	46.94
1.20	56	10	374.66±89.63	55.25
		15	491.48±108.13	53.59
		20	541.22±99.23	52.01
		25	569.17±111.88	50.70
		30	585.70±121.46	49.03
		35	595.98±113.44	47.12

Table 5: Growth rate constant for different SS

Parameter	SS=1.16	SS=1.18	SS=1.20	Mean	Standard Deviation
Order(n)	1.15	1.03	0.96	1.04	0.0975
Constant(K_G) (μm/min) $(mg/ml)^{-1}$	1.76	1.48	1.50	1.58	0.1576